PHYSICAL REVIEW A VOLUME 40, NUMBER 7 OCTOBER 1, 1989

Kinetics of droplet growth processes: Simulations, theory, and experiments

Fereydoon Family
Department of Physics, Emory University, Atlanta, Georgia 30322

Paul Meakin
Central Research and Development Department, E.I. du Pont de Nemours and Company, Wilmington, Delaware 19880-0356
(Received 19 April 1989)

The formation of a distribution of various size droplets is a characteristic feature of many systems from thin films and breath figures to fog and clouds. In this paper we present the results of our investigations of the kinetics of droplet growth and coalescence. In general, droplet formation occurs either by spontaneous nucleation or by growth from heterogeneously distributed nucleation centers, such as impurities. We have introduced two models to describe these two types of processes. In the homogeneous nucleation model droplets can form and grow anywhere in the system. The results of the simulations of the model are presented and it is shown that the droplet size distribution has a bimodal structure consisting of a monodispersed distribution of large droplets superimposed on a polydispersed distribution of smaller droplets. A scaling description for the evolution of the time-dependent droplet size distribution and its moments is presented and it is found that the scaling predictions are in excellent agreement with the simulations. A rate-equation similar to the Smoluchowski equation is also introduced for describing the kinetics of homogeneous droplet growth. The results of the simulations of the homogeneous nucleation model are also compared with the experiments on droplet growth in thin films obtained by vapor deposition of tin on sapphire substrate. It appears that this model captures the essential features of the distribution of droplets in the vapor deposition experiments. We also introduce a heterogeneous nucleation model for studying processes in which droplets only form and grow at certain nucleation centers which are initially chosen at random. Simulations, scaling theory, and a kinetic equation approach for describing the heterogeneously nucleated droplet growth model are also presented. The theoretical predictions are found to be in excellent agreement with the simulations.

I. INTRODUCTION

There is a surprisingly large number of processes where a distribution of droplets is formed by condensation of atoms and molecules from the vapor phase. An example that we have studied recently,[1-3] which will be the subject of discussion in this paper, is the formation and growth of droplets in vapor deposited thin films. In everyday experience, this type of phase transition is commonly observed in the condensation of water droplets on cold surfaces,[4,5] such as window panes, or the formation of dew on leaves and cobwebs. The condensation of liquid droplets has important technological implications for the heat-transfer industry and has been discussed extensively from the engineering point of view.[4] The formation of a distribution of various size droplets is a characteristic feature of many other systems, including breath figures,[5-7] soap bubbles,[8] fly ash particles,[9,10] microemulsion,[11] and fog, rain, and clouds.[12] In addition, understanding the growth and coalescence of droplets is of considerable interest in the study of the kinetics of nonequilibrium phase transitions[13] and spinodal decomposition.[14,15]

In this paper we present an account of our investigations of the kinetics of droplet growth in models of vapor deposited thin films[1] and droplet growth from heterogeneously nucleated centers.[2] However, our theoretical approach and the simulations are quite general and are applicable to a wide range of droplet growth processes. Our interest in this problem was initiated by experiments on vapor deposited thin films[16] and by the fact that thin films are used in an ever increasing number of scientific and industrial applications. Understanding the kinetics of their formation is a challenging problem of considerable theoretical and practical interest.[17] Frequently in thin-film deposition the initial layer condenses as discrete droplets, which grow and coalesce to form larger droplets, eventually forming a complete layer. This occurs when the binding energy of the condensate atoms to each other is greater than their binding energy to the substrate.[17] The most characteristic feature of this process is the formation of a distribution of droplet sizes that evolves with time. Figure 1(a) is an electron micrograph of vapor-deposited tin on the surface of a sapphire sample held at 230 °C. It clearly shows the distribution of tin droplets that have been formed. For comparison, in Fig. 1(b) we show the distribution of droplets obtained from a computer simulation model which we discuss in Sec. II.

Cluster growth in vapor deposition experiments is governed by two distinct mechanisms.[17] The first process is direct absorption from the vapor and the second is droplet-droplet coalescence. But in contrast to cluster-

cluster aggregation[18] processes in which clusters contact each other and combine as a result of transport processes such as diffusion, droplets join together when they touch as a result of growth. As deposition and growth continues, the separation of various droplets decreases and upon contact they coalesce to form larger droplets. The geometry of the droplets depends on the state of the coalescing particles.[17] When the substrate temperature is near or above the bulk melting point of the condensing material, droplets are liquid and spherical as in Fig. 1(a). *In situ* electron microscope observations[19] in thin-film growth have confirmed that the fusion of two liquid droplets leads to the formation of a new spherical droplet with no loss in volume. It is this type of growth that we study here.

A. Droplet growth

The most characteristic feature of any droplet growth process is shape preservation, i.e., the fact that coalescence of two droplets always leads to another droplet. The reason behind this fact is that the growth process is driven by the surface tension, which tends to minimize the surface area of the liquid droplets. Thus, when two (or more) droplets overlap [Fig. 2(a)] or touch [Fig. 2(b)], they coalesce to form a new droplet with mass conservation.

As a generalization of the growth and coalescence of spherical droplets, we assume that the droplets in our model are hyperspherical with a dimensionality D. When a droplet of radius r_1 touches or overlaps a droplet of radius r_2, a new droplet is formed, centered on the center of mass of the two original droplets, with a radius r which is given by

$$r=(r_1^D+r_2^D)^{1/D} . \tag{1}$$

If this droplet overlaps one or more other droplets, they are also coalesced and this procedure continues until no overlaps remain. Although only certain values of D are physically realizable, varying the effective dimensionality of the droplets D and the space dimension d allows us to test the dimensional dependence of various theoretical predictions.

B. Outline

The growth of a droplet occurs by condensation of small droplets that grow by absorption and coalescence with other droplets. If the condensation occurs on impurities or imperfections, the droplet is said to form by *heterogeneous nucleation*. If other substances or mechanisms do not play a role in the process, the droplets form by molecules combining together to form a small droplet which can grow spontaneously. In this case, the droplet is said to form by *homogeneous* (or spontaneous) *nucleation*.

In Sec. II we present details of the homogeneous nucleation model which we recently introduced[1] in order to describe processes where the droplets can form and grow spontaneously at any position in the system. We first present a scaling description of the model and compare the results with the simulations. We also introduce a

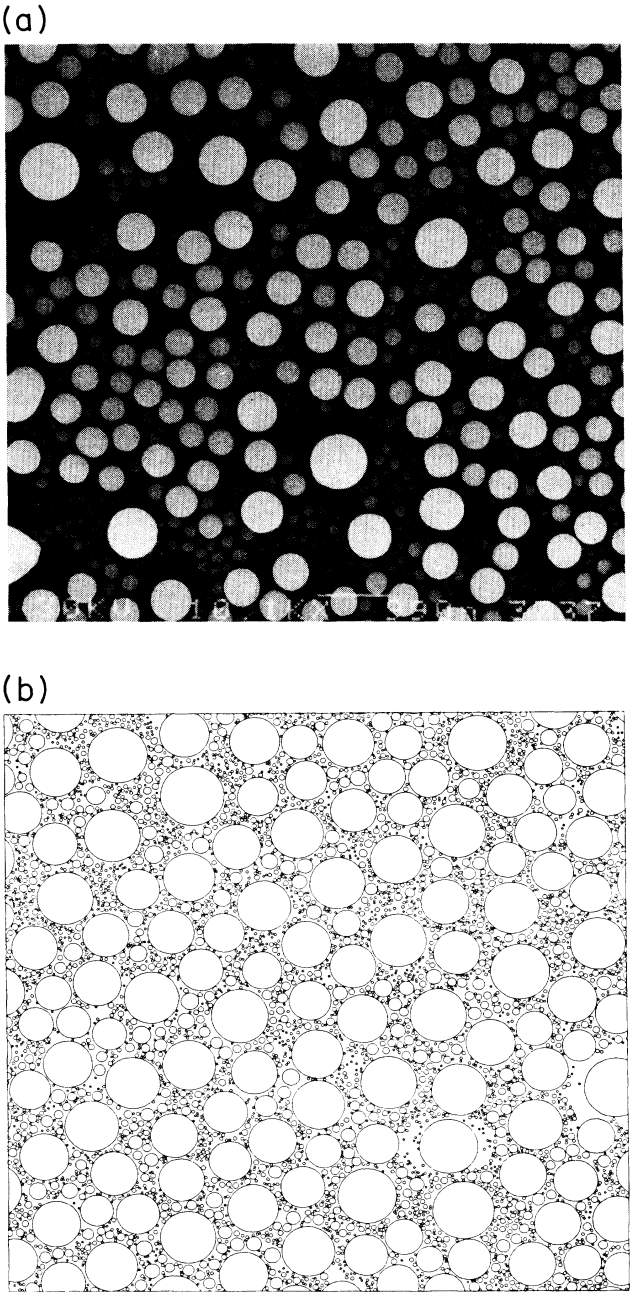

FIG. 1. (a) Comparison of an electron micrograph of tin droplets grown on a sapphire surface held at 230 °C by vapor deposition and (b) simulation carried out using the droplet deposition and coalescence model. The simulation results were obtained from a model in which three-dimensional droplets with a radius of 0.75 were randomly deposited onto a two-dimensional plane of area 512×512. The system is shown at the stage at which the mean droplet size $S(t)$ has reached a value of 1029 (in units of the mass of the deposited droplets). A 200×200 area is shown here. The uniform size of the larger droplets indicates that there exists an approximately monodispersed distribution of droplets which is superimposed on a wide distribution of smaller droplets. Depleted zones created by coalescence of droplets around large droplets are evident in both the experimental and the simulation data.

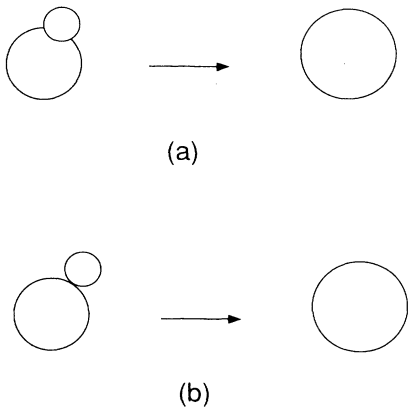

FIG. 2. Droplet coalescence and growth occurs when two or more droplets (a) overlap or (b) touch. Both mechanisms lead to the formation of a new droplet with mass conservation.

rate-equation similar to the Smoluchowski equation[20] for describing the kinetics of droplet growth. The heterogeneous nucleation model is discussed in Sec. III. We developed this model[2] to study processes in which droplets form and grow only at certain nucleation centers which are initially chosen at random. We develop both a scaling theory and a rate-equation approach for describing the kinetics of droplet growth from heterogeneously nucleated sites. We show that our theoretical predictions are in excellent agreement with simulations of the heterogeneous nucleation model. In Sec.IV, we compare the homogeneously and the heterogeneously nucleated droplet growth processes and present a brief summary of our main results.

II. HOMOGENEOUS NUCLEATION

A. Model

In the model for homogeneous nucleation, we assume that droplets can form and grow anywhere in the system. In the simulations we consider a system of size L^d to which we randomly add small droplets of fixed radius r_0. Whenever two droplets touch or overlap they are coalesced with mass conservation. The new droplet is centered on the center of mass of the two original droplets with a radius given by Eq. (1). If this droplet overlaps one or more other droplets, they are also coalesced and this procedure continues until no overlaps remain. Note that when the droplet dimension D is less than or equal to the dimension of the space d, $r \geq (r_1^D + r_2^D)^{1/d}$, so that after a finite time a single droplet forms which extends across the entire system. This phenomenon is similar to gelation and percolation.[21] For $D > d$, $r < (r_1^D + r_2^D)^{1/d}$ and there is no gelation in a finite time and the growth proceeds much in the same manner as in low-density colloidal aggregation. This implies that by using D as a variable parameter we can investigate a variety of interesting growth conditions, including percolation and aggregation of droplets. Since the experimental results in thin-film growth correspond to $D=3$ and $d=2$, in this paper we will concentrate mainly on the case $D \geq d$.

B. Droplet size distribution

The quantity that describes the kinetics of the system is the time-dependent droplet size distribution $N_s(t)$, which is the number of droplets of mass s at time t. Many quantities of interest are defined through the moments of the droplet size distribution. For example, the mean droplet size $S(t)$ is defined by

$$S(t) = \frac{\sum_s s^2 N_s(t)}{\sum_s s N_s(t)} . \tag{2}$$

A 200×200 section of a typical simulation result in which three-dimensional droplets with a radius $r_0 = 0.75$ were added at random to a surface of size 512×512, is shown in Fig. 1(b), at time t when the mean droplet size $S(t)$ has reached a mass of 1029 particles. Comparison of Figs. 1(a) and 1(b) shows that there are many similarities between the experimental data and our simulation. For example, the existence of depleted zones around large droplets is evident in both figures. These depleted regions are left behind by coalescence of two (or more) large droplets, before new particles have had a chance to accumulate there. In Fig. 3 we show 200×200 sections of the distribution of droplets at four different stages during the formation of droplets where three-dimensional drops of radii 0.75 were added randomly to a 512×512 substrate. Figures 3(a)–3(d) show the distribution of droplets at the instant at which the mean droplet size S has reached values of 10.4, 105, 1029, and 10177, respectively. As time increases the average droplet size increases. The depleted zones left behind by coalescence of droplets is evident in these figures as well.

The distribution of droplets shown in Figs. 1 and 3 have two novel features. One of the characteristics of all these figures is the existence of a distribution of large droplets of nearly equal size, which can be distinguished from the smaller droplets forming the background. The second feature is the distribution of the smaller droplets, which in contrast to the monodispersed distribution of large droplets, consists of an inhomogeneous and polydispersed distribution of all sizes. We have observed similar types of bimodal distributions in one-, two- and three-dimensional simulations for droplets with $D > d$.

The existence of the two parts in the droplet size distribution implies that there are two distinct mechanisms controlling the formation of small and large droplets. The small droplets are formed by spontaneous nucleation, in a manner similar to aggregation processes with a source.[22] As it was also found in the case of aggregation,[22] the presence of a source leads to a polydispersed distribution that is quite broad, having a power-law decay with droplet mass. In fact, in the presence of a sink for large droplets the size distribution goes to a steady state. The sink in this case is the large droplets. Once the droplets reach a certain characteristic size, they coalesce and form large droplets that continue to grow and coalesce and form a monodispersed size distribution. The charac-

teristic size of the droplets depends on d and D. The bell-shaped distribution for large droplets is similar to diffusion-limited aggregation, where the process is dominated by aggregation of similar size clusters leading to a monodispersed distribution.

Figure 4 shows three stages in a simulation in which two-dimensional droplets were deposited onto a two-dimensional substrate ($d=D=2$). Figures 4(a)–4(c) show the distribution of droplets at three different stages characterized by a mean droplet size S of 61.2, 423.9, and 1888, respectively. It is interesting to compare the distribution of the droplets in Fig. 4 with those shown in Figs.

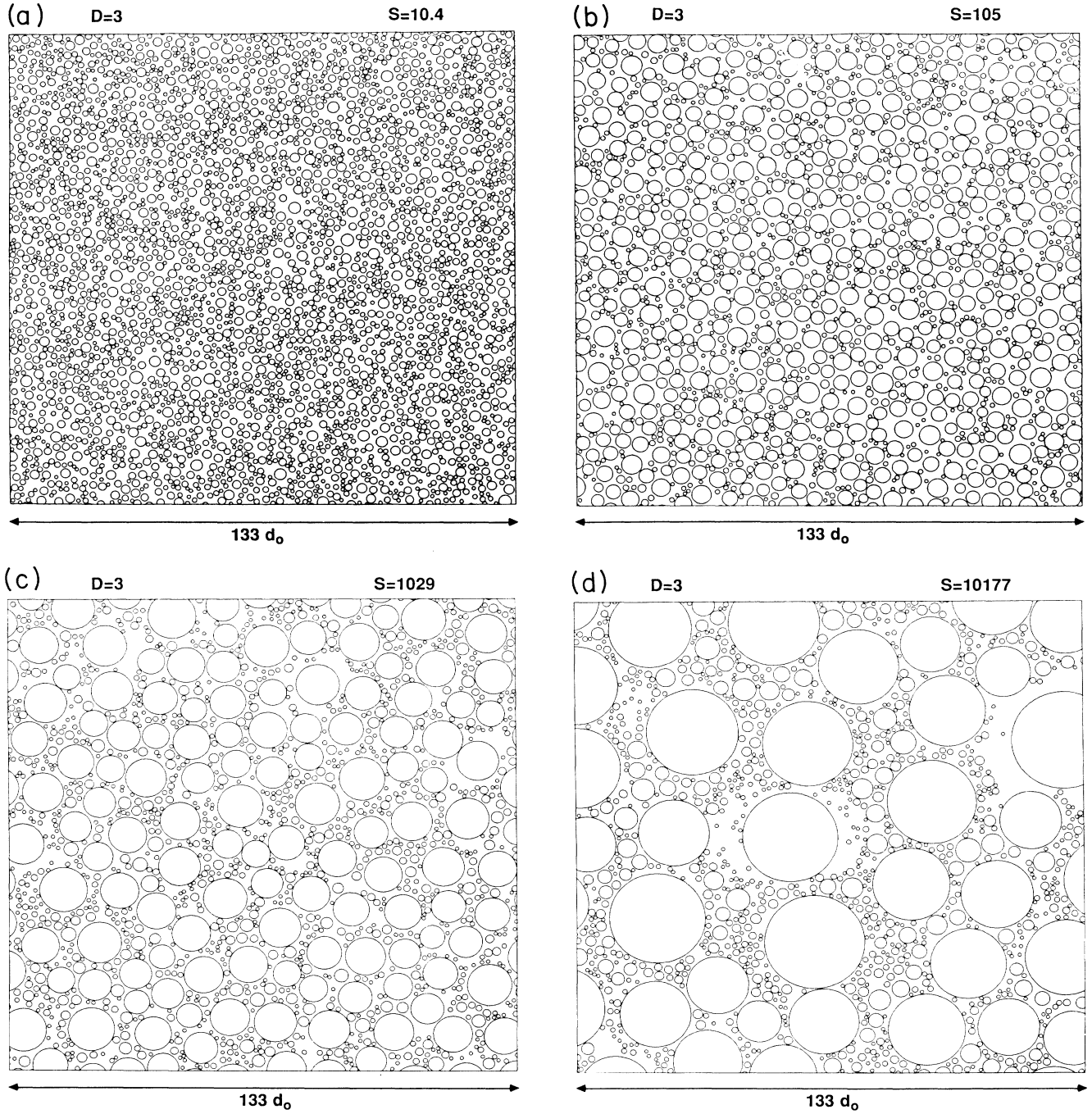

FIG. 3. Four stages in a simulation in which three-dimensional droplets were randomly deposited onto a two-dimensional surface. (a)–(d) show 200×200 areas taken from simulations carried out on a 512×512 substrate (with periodic boundary conditions) at the instant at which the mean droplet size $S(t)$ reached values of 10.4, 105, 1029, and 10 177, respectively. The droplet size distribution consists of a monodispersed distribution of larger droplets superimposed on a highly polydispersed distribution of smaller droplets in the background. We find bimodal distribution of droplets in $d=1$, 2, and 3 for the cases where $D>d$.

1 and 3. Note that in contrast to the bimodal distributions observed in Figs. 1 and 3, here the droplets form a highly polydispersed distribution of droplets of all sizes. This transition from a bimodal distribution to a single polydispersed distribution occurs in all dimensions as the droplet dimension D becomes equal to the space dimension d. We will provide quantitative analysis of these observations in Secs. II C–II E.

C. Scaling theory

In order to develop a description of the droplet size distribution, in analogy with the scaling approach for ag-

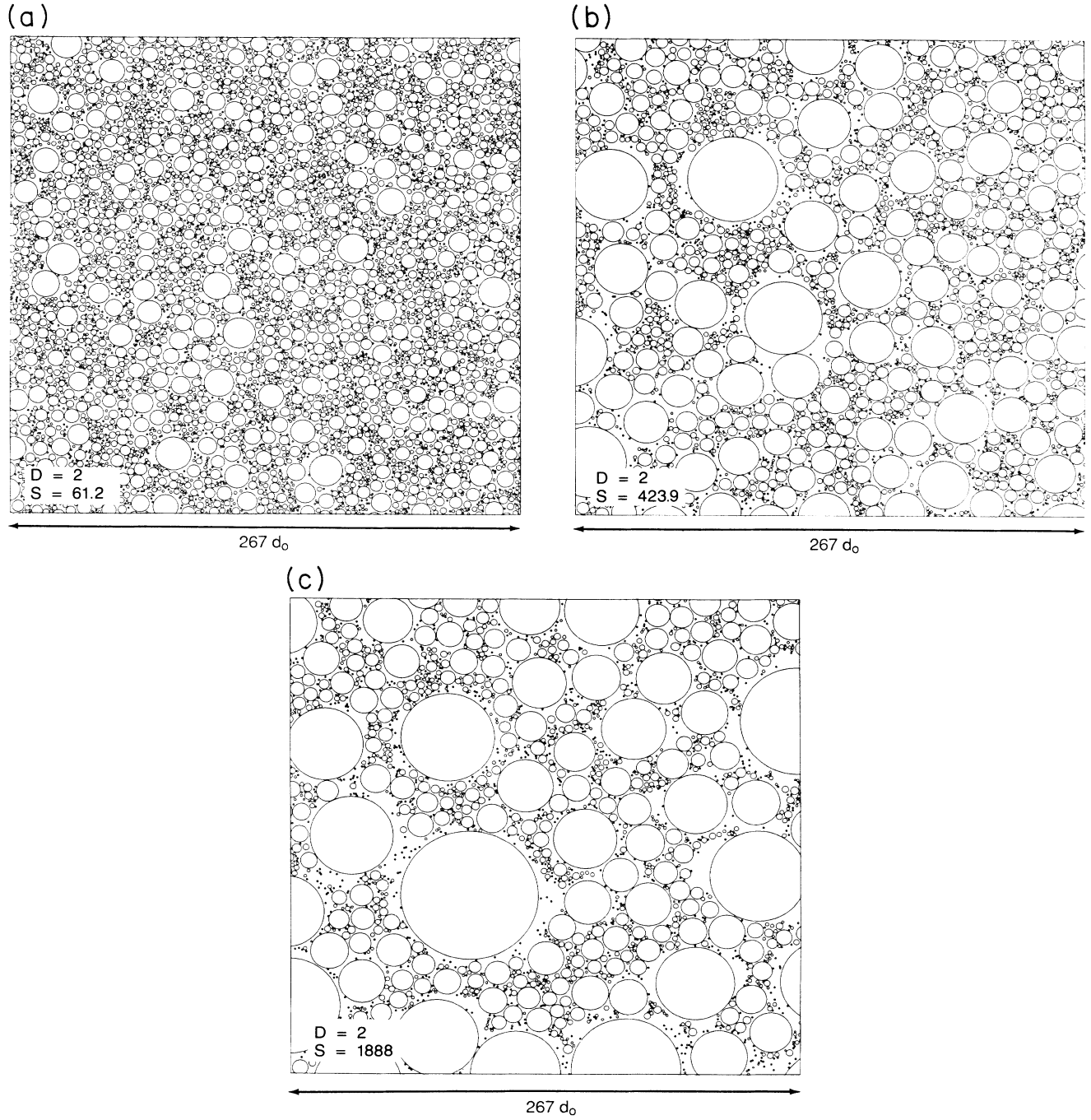

FIG. 4. Three stages in a simulation in which two-dimensional droplets were deposited onto a two-dimensional substrate. (a)–(c) show the distribution of droplets at three different stages characterized by mean droplet size $S(t)$ of 61.2, 423.9, and 1888, respectively. Note that in contrast to the distributions shown in Figs. 1 and 3, the droplet size distribution here is highly polydispersed. We find similar results in $d=1$, 2, and 3 for the case $D=d$.

gregation processes,[23] we assume that the mean cluster size $S(t)$ is the only characteristic cluster size in the system. Since the mean droplet size increases with time, we assume that $S(t)$ and the mean droplet radius $R(t)=S(t)^{1/D}$ diverge as

$$S(t)\sim t^{z},\quad R(t)\sim t^{z/D}\ , \tag{3}$$

where the dynamic exponent z must depend on both d and D. The total number of droplets in the system $N(t)$ is expected to decrease with an exponent z' as

$$N(t)=\sum_{s} N_s(t)\sim t^{-z'}\ . \tag{4}$$

We generalize the scaling description of the cluster size distribution in aggregation processes and write[1]

$$N_s(t)\sim s^{-\theta} f(s/S(t))\ . \tag{5}$$

The bimodal form of $N_s(t)$ is reflected in the form of $f(x)$, which consists of two parts:

$$f(x)=x^{(\theta-\tau)}g(x)+h(x)\ . \tag{6}$$

The function $g(x)$ goes to a constant for small x and decays faster than any power of x for large x. The second part of the distribution is reflected in the function $h(x)$, which is a bell-shaped function with a peak centered about $x=1$. Therefore the exponent τ describes the decay of the distribution for small droplet masses and θ describes the scaling of the full distribution.

A qualitative test of the scaling ideas is provided by Figs. 5 and 6 in which the distribution of the clusters is scaled according to Eq. (5) by plotting the droplet size distribution at a scale proportional to $S^{1/D}$. Figure 5 shows four stages in a simulation in which three-dimensional droplets were deposited onto a two-dimensional substrate. This figure shows portions of the system at four different stages corresponding to mean cluster sizes $S(t)$ of 54, 428, 3237, and 26 118. Each part of the figure is shown at a scale proportional to $S^{1/3}$ to illustrate the rapid approach to a scaling regime. Figure 6 shows three stages in a simulation in which two-dimensional droplets were deposited onto a two-dimensional substrate. The upper left, upper right, and lower left parts of the figure show the system at stages corresponding to mean droplet sizes $S(t)$ to 124, 723, and 2632. In each case, a scale proportional to $S^{1/2}$ has been used to illustrate the self-similarity of the distribution. The lower-right part of the figure shows the system at the $S=2632$ stage with small droplets removed. Note that all the scaled distributions in Fig. 6 are polydispersed, in agreement with our previous discussion of the droplet size distribution for $D>d$ (Fig. 3) and $D=d$ (Fig. 4).

The time evolution of the droplet size distribution $N_s(t)$ at 16 stages in the deposition of three-dimensional droplets onto a two-dimensional substrate is shown in Fig. 7. These results were obtained from 29 simulations. In each simulation, 2.3×10^{6} droplets with a radius of 0.75 were deposited onto a substrate of area 512×512 (with periodic boundary conditions). Note the bimodal shape of the distribution in the later stages of the growth. The scaling of the droplet size distributions for the case $D=3$, $d=2$ is shown in Fig. 8. Figure 8(a) shows the

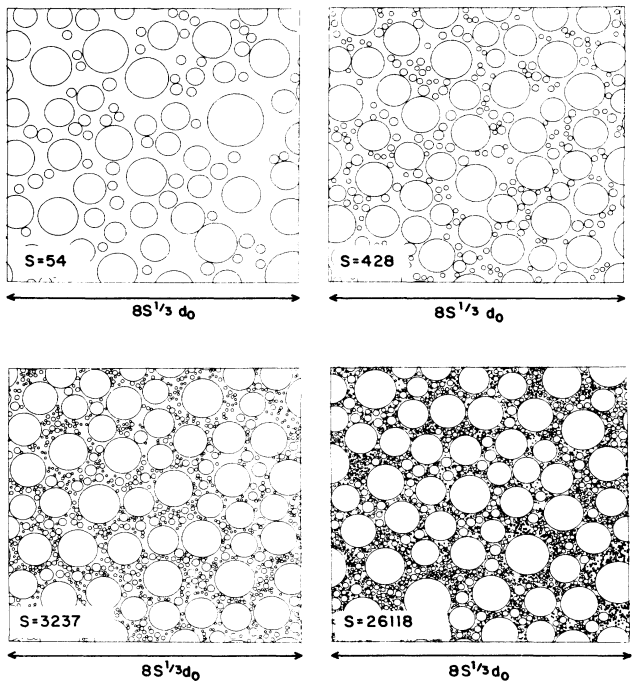

FIG. 5. Four stages in a simulation in which three-dimensional droplets were deposited onto a two-dimensional substrate. This figure shows portions of the system at four different stages corresponding to mean cluster sizes $S(t)$ of 54, 428, 3237, and 26 118. Each part of the figure is shown at a scale proportional to $S^{1/3}$ to illustrate the rapid approach to a scaling regime.

droplet size distribution at the last five stages in the simulations used to obtain Fig. 7. Figure 8(b) shows how these size distributions can be scaled onto a common scaling function using the scaling form given in Eq. (5) with a scaling exponent θ of $\frac{5}{3}$, which we obtain from theoretical arguments in Sec. II D [Eq. (10)]. The scaling function obtained in Fig. 8 agrees with the form proposed in (6) and the nonzero slope for small values of the argument of the scaling function indicates that $\theta-\tau>0$.

The condensation of liquid droplets on a thread, such as the formation of dew on a cobweb, presents an interesting physical system for the study of droplet growth. Figure 9 shows the droplet size distributions obtained from simulation of droplet deposition and coalescence on a line ($d=1$). Figure 9(a) shows results for two-dimensional droplets and Fig. 9(b) shows the results for three-dimensional droplets. The cluster size distributions are shown at late stages in the simulation (close to the scaling limit). In analogy with the two-dimensional results, the droplet size distribution has a bimodal shape since $D>d$. Figure 10 shows the scaling of the droplet size distributions shown in Fig. 9. The scaling form given in Eq. (5) was used with a scaling exponent θ of $(D-d)/D$ [Eq. (10)]. The figures show that the form of the scaling function $f(x)$ agrees with (6).

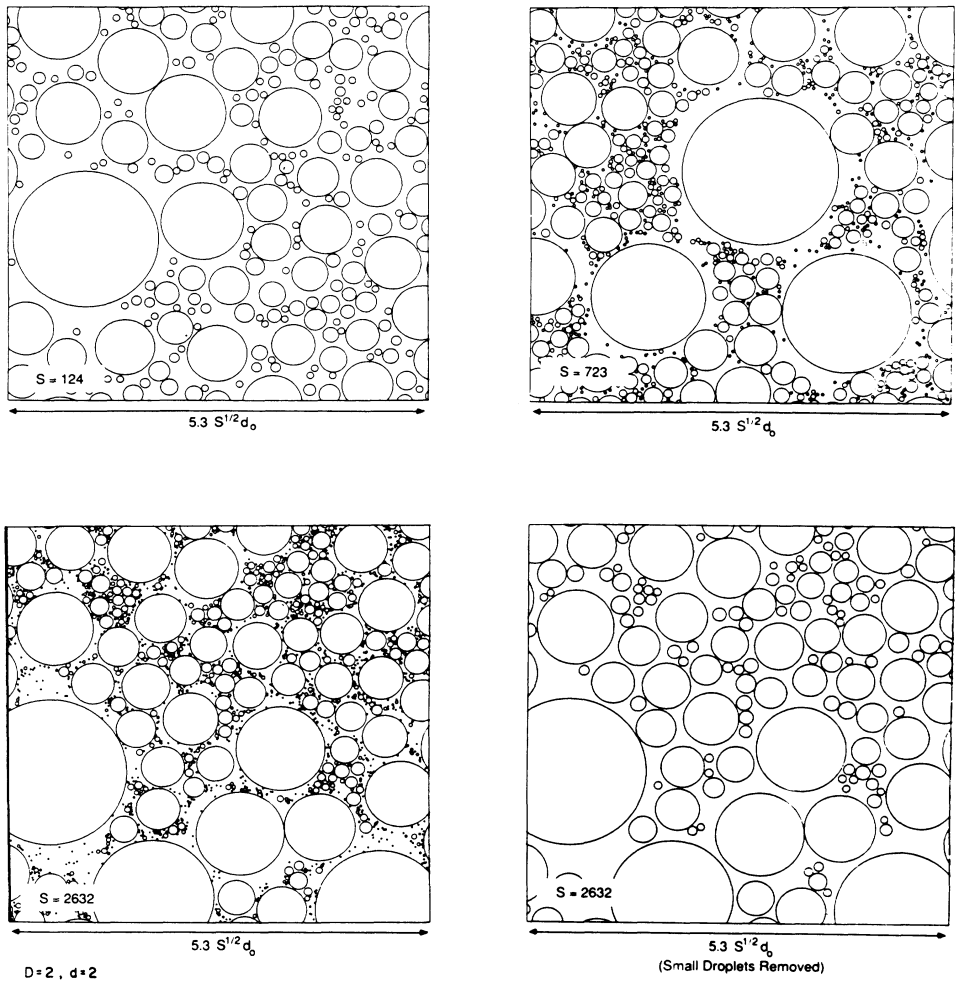

FIG. 6. Three stages in a simulation in which two-dimensional droplets were deposited onto a two-dimensional substrate. The upper-left, upper-right, and lower-left parts of the figure show the system at stages corresponding to mean droplet sizes $S(t)$ of 124, 723, and 2632. In each case, a scale proportional to $S^{1/2}$ has been used to illustrate the self-similarity of the distribution. The lower-right part of the figure shows the system at the $S=2632$ stage with small droplets removed.

D. Exponents

In this section we calculate the exponents θ and z exactly. Since the total mass in the system is not constant, the exponent θ depends on d and D and does not have a *superuniversal* value of 2 as in aggregation processes.[23,24] However, in the droplet growth problem, the time t is equal to the total number of particles that have been added to the system. Using (3) and (5) we can write

$$\rho = t = \sum_s s N_s(t) \sim \int ds\, s^{1-\theta} f(s/S(t)) \sim S^{2-\theta} \times \int dx\, x^{1-\theta} f(x) \sim t^{z(2-\theta)}, \qquad (7)$$

where ρ is the density of the system. Since the second integral on the right-hand side of (7) is independent of t, (7) implies that

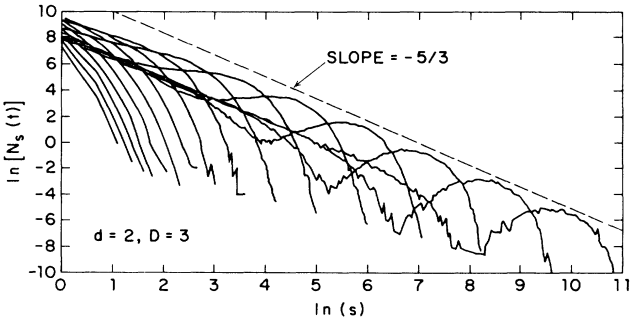

FIG. 7. Droplet size distributions, $N_s(t)$ at 16 stages in the deposition of three-dimensional droplets onto a two-dimensional substrate. These results were obtained from 29 simulations. In each simulation, 2.3×10^6 droplets with a radius of 0.75 were deposited onto a substrate of area 512×512 (with periodic boundary conditions).

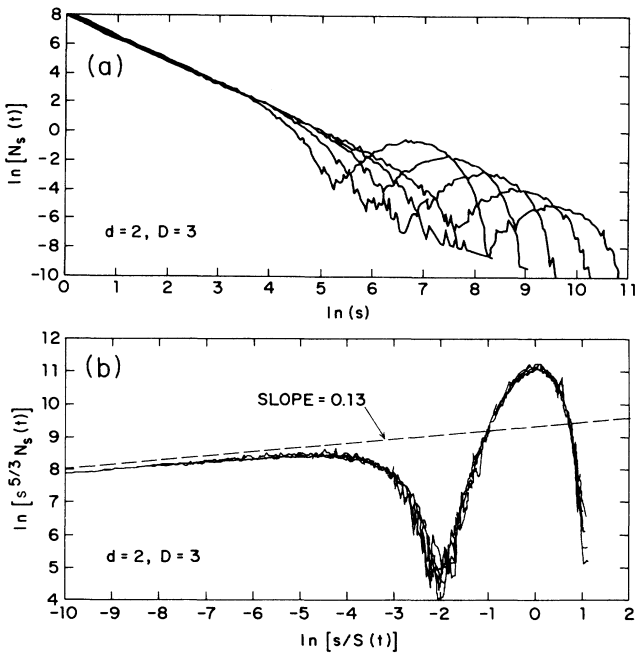

FIG. 8. Scaling of the droplet size distributions for the $D=3$, $d=2$ case. (a) shows the droplet size distribution at five late stages during the simulation taken from the simulations used to obtain Fig. 7. (b) shows how these size distributions can be scaled onto a common scaling function using the scaling form given in Eq. (5) with a scaling exponent θ of $\frac{5}{3}$ given by Eq. (10). The nonzero slope for small values of the argument of the scaling function indicates that $\theta-\tau>0$.

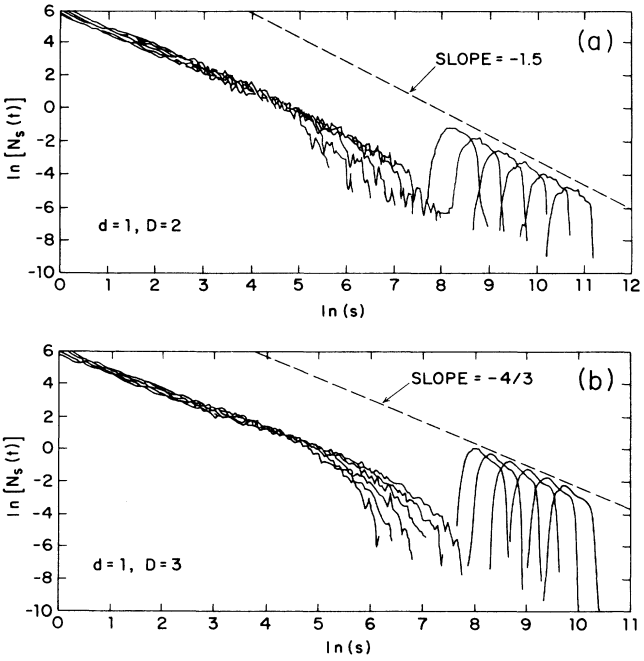

FIG. 9. Droplet size distributions obtained from simulation of droplet deposition and coalescence on a line ($d=1$). (a) shows results for two-dimensional droplets and (b) shows results for three-dimensional droplets. The cluster size distributions are shown at late stages in the simulation (close to the scaling limit).

$$\theta+1/z=2\ . \tag{8}$$

Therefore $\theta\leq 2$ because $z>0$.

In order to determine θ we note that the fraction of the volume Φ occupied by the droplets is given by

$$\Phi=\sum_s r^d N_s(t)\sim\int ds\, s^{d/D-\theta} f(s/S(t))\sim S^{1+d/D-\theta}. \tag{9}$$

Since Φ cannot diverge, then

$$\theta=1+d/D\ . \tag{10}$$

For a gelling system $\theta>2$ and therefore Eq. (10) confirms our earlier observation that for $d>D$ the system will percolate.[21] Note that when $d=D$, $\theta=2$. Substituting this in (8) we find that as $d\to D$, $z\to\infty$, implying that the mean droplet size diverges exponentially, indicating a percolation transition. This is consistent with our earlier observations that for $d=D$, the system percolates after a finite time, and the droplet size distribution is polydispersed with a power-law decay of the distribution with droplet mass (cf. Figs. 4 and 6).

Using (10) in (8) we find $z=D/(D-d)$. We can obtain this result directly by assuming that R is the only relevant length in the system. Let us define the correlation function $G(r)$ to be the probability that a site at distance r from an occupied site in a finite droplet is also occupied and belongs to the same droplet. In terms of $G(r)$, the mean cluster size $S(t)$ is given by

$$S(t)=\int d^d r\, G(r)\ . \tag{11}$$

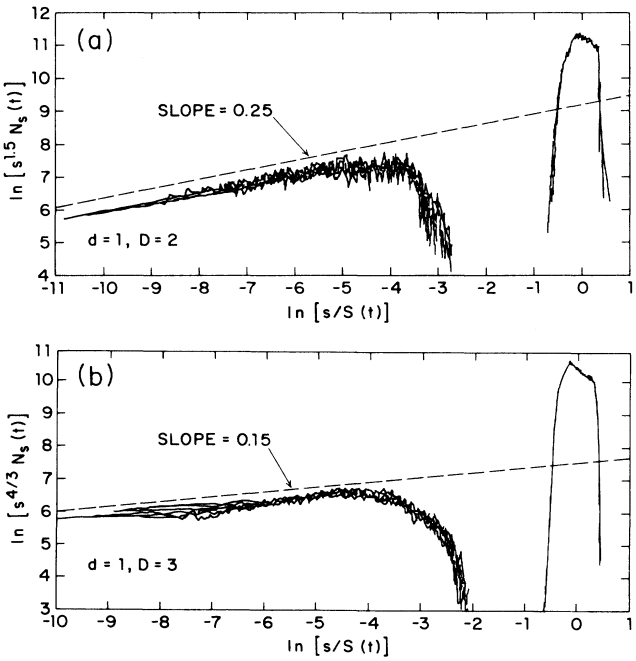

FIG. 10. Scaling of the droplet size distributions shown in Fig. 9. The scaling form given in Eq. (5) was used with a scaling exponent θ of $(D-d)/D$ [Eq. (10)]. The figures show that the scaling function agrees with Eq. (6).

Assuming that $R(t)$ is the only length in the problem, $G(r)$ can be written in the form

$$G(r)=\rho k(r/R) , \tag{12}$$

where $k(x)$ is a scaling function that depends only on the ratio of r to the mean cluster radius R. Inserting (12) in (11), and using (3) and (7), we find

$$S(t)=\rho R^d \int d^d x\, k(x) \sim t^{1+zd/D} . \tag{13}$$

In comparing (13) with (3) we find

$$z=D/(D-d) . \tag{14}$$

As noted before, for $D=d$, $\theta=2$, $z\to\infty$, and $S(t)$ grows exponentially. This implies that the droplet size distribution is polydispersed as found in Figs. 4 and 6.

As it was pointed out before,[24,25] the value of the exponent z' depends on the exponent τ. We follow the approach of Refs. 24 and 25, and using (6) and (4), we find

$$N(t)=\begin{cases} t^{-z(\theta-1)} & \text{for } \tau<1 \\ t^{-z(\theta-\tau)} & \text{for } \tau>1 \end{cases} . \tag{15}$$

In the droplet growth model τ is greater than 1. This implies that[26,27]

$$z'=z(\theta-\tau) . \tag{16}$$

Figure 11(a) shows the growth of the mean droplet size $S(t)$ and time dependence of the total number of droplets $N(t)$ obtained from the simulations used to generate Figs. 7 and 8. This figure indicates that in the asymptotic limit ($t\to\infty$), the mean droplet size grows as t^z where the exponent z has a value consistent with the theoretical value of 3 given by Eq. (14). The decrease in the number of droplets as ($t\to\infty$) also appears to have an algebraic time dependence [Eq. (4)] with an exponent z' of about 0.26. This result and the values of z' for other models are listed in Table I and are found to be in agreement with (16). Figures 11(b) and 11(c) show results obtained for the growth of $S(t)$ and the decay of $N(t)$ from the simulations used to generate Figs. 10(a) ($D=2$, $d=1$) and 10(b) ($D=3$, $d=1$), respectively.

In Table I we list the numerical estimates of the exponents z, z', and τ for various values of the droplet dimension D and space dimension d. The theoretically predicted values for z are given in the parentheses. The numerical values of the exponent z are in good agreement with the theoretical predictions. The results for z' are also in relatively close agreement with (16). In all cases we have obtained convincing data collapsing of the droplet size distribution using the theoretical values of $1+d/D$ for the exponent θ. The statistical uncertainties in the values of the exponents are quite small, but it is difficult to determine the systematic errors arising from corrections to the asymptotic scaling behavior. In most cases the overall agreement with theoretical predictions indicates that these uncertainties are also very low.

In most of our simulations the centers of the droplets are located on the d-dimensional substrate. In the case $D=3$, $d=2$, this could be interpreted in terms of hemispherical droplets lying on a plane surface. We have also carried out simulations in which three-dimensional spherical droplets sit on a two-dimensional substrate. In this model large droplets can overshadow smaller droplets. We find that the exponents (z, z', θ, and τ) associated with this model are the same as those found for hemispherical droplets. In general, we do not expect that the values for these exponents will be sensitive to such details but we have not carried out intensive simulations to test this idea.

E. Kinetic equation approach: Mean-field theory

The traditional method for studying the kinetics of aggregation processes is to use the Smoluchowski rate-

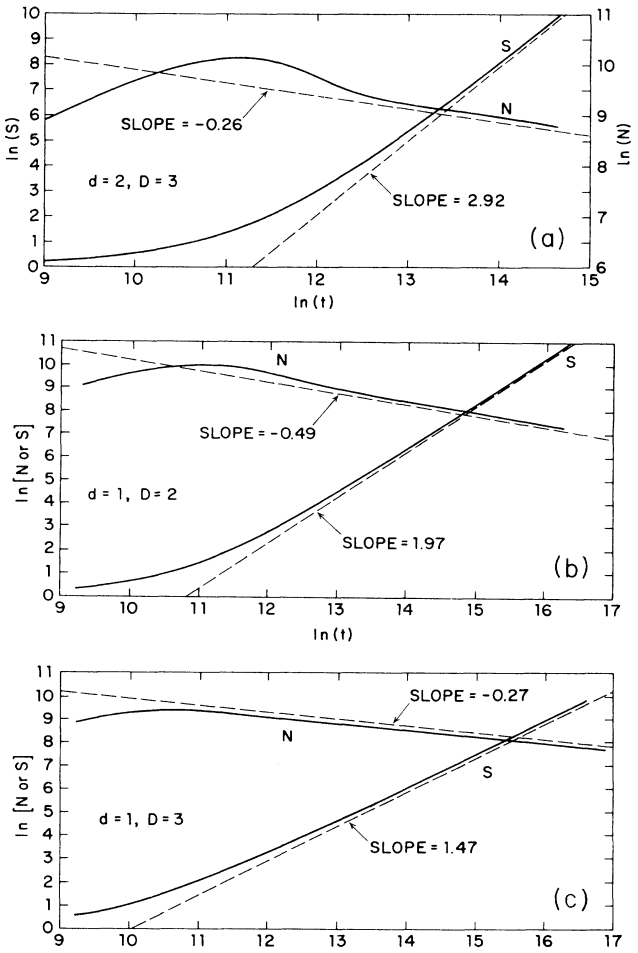

FIG. 11. (a) shows the growth of the mean droplet size $S(t)$ and time dependence of the total number of droplets $N(t)$ obtained from the simulations used to generate Figs. 7 and 8. This figure indicates that in the asymptotic limit ($t\to\infty$), the mean droplet size grows as t^z where the exponent z has a value consistent with the theoretical value of 3 given by Eq. (14). The decrease in the number of droplets as ($t\to\infty$) also appears to have an algebraic time dependence [Eq. (4)] with an exponent z' of about 0.26. (b) and (c) show results obtained for the growth of $S(t)$ and the decay of $N(t)$ from the simulations used to generate Figs. 10(a) ($D=2$, $d=1$) and 10(b) ($D=3$, $d=1$), respectively.

equation approach.[20] Similarly, for the growth and coalescence of droplets we can write the following kinetic equation:

$$\frac{dN_s}{dt}=\tfrac{1}{2}\sum_{i+j=s}K_{ij}N_iN_j-N_s\sum_{j=1}^{\infty}K_{sj}N_j +K'_{s-1,1}N_{s-1}-K'_{s,1}N_s\ , \tag{17}$$

where K_{ij} is the rate coefficient for coalescence of a droplet of size i with a droplet of size j, and $K'_{i,1}$ is the rate of growth of droplets of size i due to absorption of monomers. The main advantage of the kinetic equation approach is that it provides a simple physical interpretation of the temporal evolution of the size distribution. The first term on the right-hand side is the rate at which droplets of size s are formed by aggregation of droplets of size i and j to form droplets of size s. The second term is the rate at which droplets of size s disappear by coalescence with droplets of size j. The third and fourth terms describe the growth of the droplets by absorption of monomers from the vapor. The third term gives the rate at which droplets of size $s-1$ grow to form droplets of size s. The last term gives the rate at which the number of droplets of size s disappear when they absorb a monomer and form droplets of size $s+1$.

The kinetic equation (17) provides a mean-field description of the growth and coalescence of droplets, because spatial fluctuations in the density of the droplets is neglected. Except for special cases, the kinetic equation cannot be solved for the physically interesting forms of the K_{ij}. However, using the dynamic scaling approach,[23] it is possible to obtain results without solving the kinetic equation directly. According to the scaling assumption, the rate equation (17) is invariant under the transformations

$$\begin{aligned} &s\to bs\ ,\\ &t\to b^{1/z}t\ ,\\ &K_{ij}\to b^{-\lambda}K_{ib\,jb}\ ,\\ &N_s(t)\to b^{-\theta}N_{sb}(b^{1/z}t)\ , \end{aligned} \tag{18}$$

where b is a scale factor and λ is the degree of homogeneity of the reaction kernel. Using these transformations in (17) we find the relation

$$\theta-\frac{1}{z}=1+\lambda\ . \tag{19}$$

TABLE I. Effective values obtained for the exponents z, z', and τ from the deposition and coalescence models (homogeneous nucleation model). The theoretical value of z is given in parentheses. In all cases a convincing data collapse of the droplet size distributions could be obtained using the theoretical values for θ ($\theta=1+d/D$).

d	D	z	z'	τ	d	D	z	z'	τ
1	1.5	2.94 (3.0)	0.51	1.48	2	4	1.84 (2.0)	0.195	1.45
1	2	1.97 (2.0)	0.62	1.19	2	5	1.61 (1.67)	0.151	$\tau\simeq\theta$
1	2.5	1.64 (1.67)	0.38	1.13	2	8	1.26 (1.33)	0.083	$\tau\simeq\theta$
1	3	1.47 (1.50)	0.27	1.18	2	16	1.06 (1.14)	0.047	$\tau\simeq\theta$
1	3.5	1.35 (1.40)	0.235	$\tau\simeq\theta$	2	24	1.01 (1.09)	0.020	$\tau\simeq\theta$
1	4	1.28 (1.33)	0.18	$\tau\simeq\theta$	2	∞	0.99 (1.0)		$\tau\simeq\theta$
1	8	1.10 (1.14)	0.079	$\tau\simeq\theta$	3	3.5	5.15 (6.0)		
1	16	1.00 (1.07)	0.035	$\tau\simeq\theta$	3	4	3.64 (4.0)		
1	24	1.01 (1.04)	0.020	$\tau\simeq\theta$	3	4.5	2.70 (3.0)	0.125	$\tau\simeq\theta$
1	∞	0.99 (1.0)	~ 0	$\tau\simeq\theta$	3	5	2.29 (2.50)	0.113	$\tau\simeq\theta$
2	2.5	4.3 (5.0)			3	16	1.12 (1.14)	0.032	$\tau\simeq\theta$
2	3	2.92 (3.0)	0.26	1.54	3	32	1.08 (1.07)	0.017	$\tau\simeq\theta$
2	3.5	2.08 (2.33)	0.24		3	∞	1.00 (1.00)	0.001	$\tau\simeq\theta$

Combining (8) with (19) we find

$$z=\frac{2}{1-\lambda}, \quad \theta=\frac{3+\lambda}{2} . \tag{20}$$

Substituting the exact values of θ and z from (10) and (14), respectively, in (20) we find

$$\lambda=\frac{2d}{D}-1 . \tag{21}$$

This is a new nontrivial result for the degree of homogeneity of the reaction kernel in droplet coalescence and growth. It would be instructive to determine the kernel directly using techniques similar to those used in the study of cluster-cluster aggregation[18] in order to test relation (21).

III. HETEROGENEOUS NUCLEATION

A. Model

In order to describe droplet growth and coalescence with heterogeneous nucleation we have developed a model where initially, there is a fixed number of nucleation sites in the system. The simulations are started by placing N_0 droplets of diameter d_0 in a d-dimensional system of size L^d such that there is no overlap between the droplets. In general, droplets grow by two distinct mechanisms. The first process is direct absorption from the vapor and the second is droplet coalescence. In a uniform vapor density, every droplet grows at a rate that is proportional to its surface area. As a generalization of this scenario, we assume that the droplet radii grow as

$$\frac{dr}{dt} \propto r^{\omega} , \tag{22}$$

where ω is an arbitrary exponent which can be varied in the model in order to test the theoretical predictions. In each time step in the simulations, the radius of each of the droplets is increased according to (22) using the formula

$$r'=(r^{\xi}+\delta\xi)^{1/\xi} , \tag{23}$$

where r' is the new radius, $\xi=1-\omega$, and δ is a small number. As the growth of the droplets continues, the separation of various droplets decreases and—upon contact—droplets coalesce to form larger droplets. We assume that all the nucleation events occur at the start of the growth and coalescence process and that after coalescence of two (or more) droplets no new nucleation sites are exposed. In each time step, droplets are examined for possible overlaps and overlapping droplets are coalesced with mass and center-of-mass conservation using relation (1).

Figure 12 shows the distribution of droplets at three stages in a simulation in which three-dimensional droplets grow and coalesce on a two-dimensional surface with a growth exponent ω of $\frac{1}{2}$. The simulations were carried out starting with $N_0=20\,000$ nuclei with a diameter d_0 of 1.5 on a surface of area 512×512. Figures 12(a)–12(c) show a 200×200 ($133d_0\times133d_0$) area at the stage where the mean droplet size S has grown to 10.3, 1036, and 108 744, respectively. These figures show that unlike the case of homogeneous nucleation the distribution is asymptotically quite monodispersed with no power-law background.

Figure 13 shows the results obtained from a simulation similar to the one illustrated in Fig. 12 except that the dimensionality D of the droplets is 2. Figures 13(a)–13(c) show a portion of the system at the stages at which the mean cluster size S has reached values of 103, 1989, and 10 156, respectively. Note that unlike the case $D>d$, here the distribution is polydispersed. The reason for the transition from the monodispersed distribution to the polydispersed case is similar to the homogeneous nucleation case discussed in Sec. II.

Figure 14 shows three stages in a simulation in which three-dimensional droplets were grown on a two-dimensional substrate with a growth exponent ω of 0. The simulation was stopped and the droplet distribution recorded at the stages corresponding to mean droplet sizes S of 11.5, 1011, and 101 631 in Figs. 14(a)–14(c), respectively. Since $D>d$, the distribution is monodispersed, as expected.

B. Scaling theory and exponents

We can describe the process of droplet growth with heterogeneous nucleation in a way very similar to our approach for homogeneous nucleation, using the scaling form (5). In order to show qualitatively that the droplet size distribution can be scaled according to (5), in Fig. 15 we have plotted the distributions at three different times during the growth, but we have rescaled all the lengths in such a way that the system size in all three figures is equal to $8d_0S^{1/3}$, where S is the mean droplet size. It is clear from these figures that the droplet size distribution is quite self-similar. Figure 16 shows three more distributions obtained from three different versions of heterogeneously nucleated droplet growth and coalescence model. Figures 16(a) and 16(b) show results from simulations with $D=3$ and $d=2$ with growth exponents ω of 0 and 0.5, respectively. Figure 16(c) shows the droplet size distribution for simulations with $D=2$ and $d=1$ with $\omega=0$. The scaling of the droplet size distributions shown in Fig. 16 is demonstrated in Fig. 17. Here the scaling form given in Eq. (5) was used with a scaling exponent θ of $(D+d)/D$ [Eq. (26)]. We have obtained equally excellent scaling plots for other values of ω and D in $d=1$, 2, and 3.

We now determine the exponents θ, z, and z' exactly for the case of heterogeneously nucleated droplets. Although we can follow exactly the same line of reasoning as in the case of homogeneous nucleation, we give here a slightly different derivation of the results to show the versatility of the scaling approach. As before, the only assumption in our calculation is that the mean droplet radius $R(t)$ is the only characteristic length in the problem. For the mass density ρ we can write

$$\rho \sim R^{D-d} \sim t^{z(D-d)/D} . \tag{24}$$

Using the scaling form (5) in the definition of ρ, we get

$$\rho=\sum_s sN_s(t)\sim\int ds\, s^{1-\theta}f(s/S(t))\sim S^{2-\theta}\times\int dx\, x^{1-\theta}f(x)\sim t^{z(2-\theta)}\,. \quad (25)$$

In comparing (24) with (25) we find

$$\theta=1+\frac{d}{D}\,. \quad (26)$$

This expression is the same as the one given in (10) for homogeneous nucleation because the arguments leading to (10) are independent of the rule for the growth of the

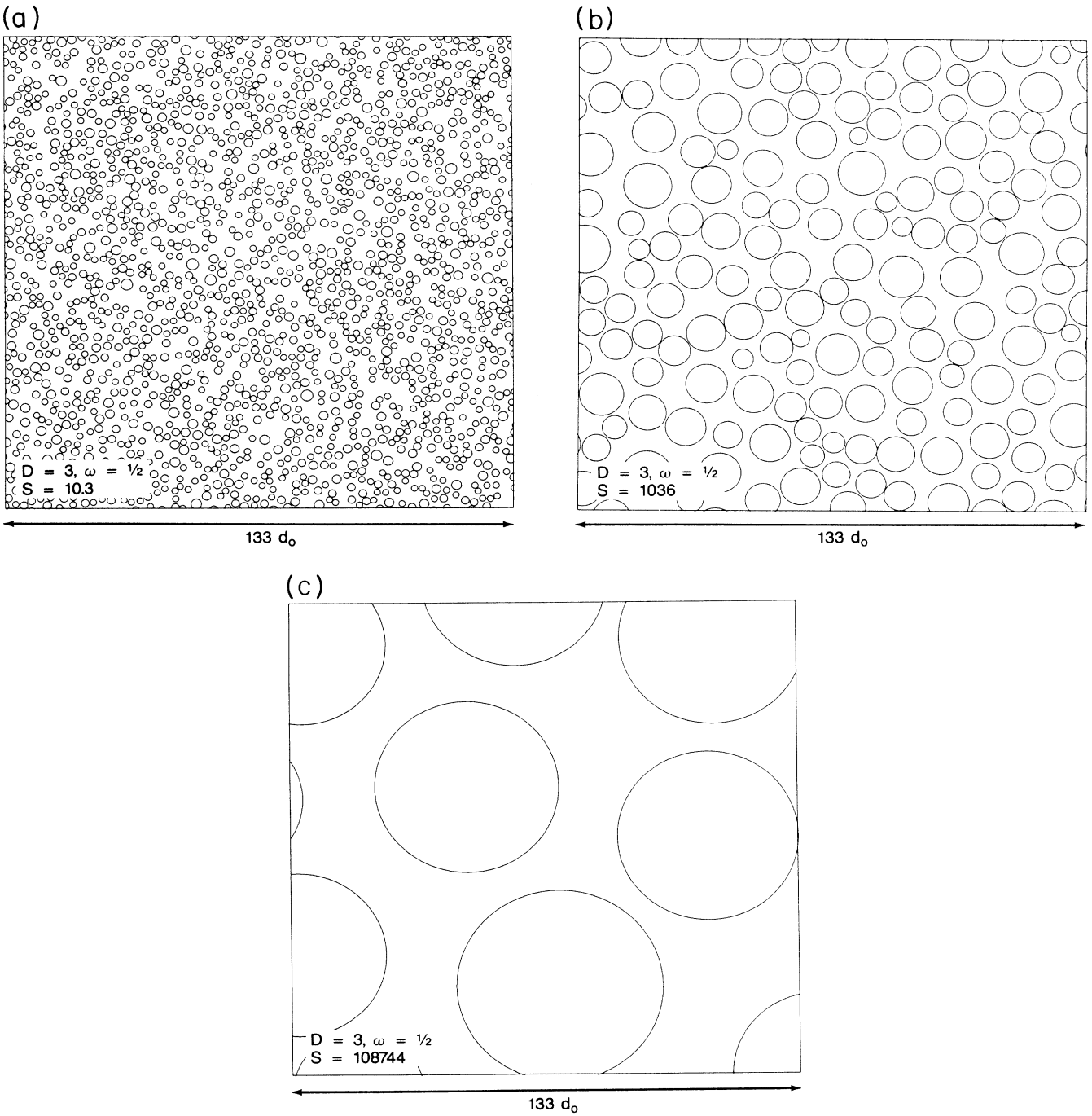

FIG. 12. Three stages in a simulation in which three-dimensional droplets grow and coalesce on a two-dimensional surface with a growth exponent (ω) of $\frac{1}{2}$. (a)–(c) show a 200×200 ($133d_0\times133d_0$) area at the stage where the mean droplet size (S) has grown to 10.3, 1036, and 108 744, respectively. The simulations were carried out starting with 20 000 nuclei with a diameter d_0 of 1.5 on a surface of area 512×512.

individual droplets.

In order to determine the growth-law exponent z, we note that our scaling assumption indicates that the growth of the mean droplet radius is governed by (22), with or without coalescence. This implies that

$$R(t)\sim t^{1/(1-\omega)} . \tag{27}$$

Using the fact that $S(t)\sim R(t)^D$, from (3) and (27) we find

$$z=\frac{D}{1-\omega} . \tag{28}$$

Alternatively, we can obtain this expression for z by substituting for R from (27) and for ρ from (25) in (13).

Since the scaling function $f(x)$ goes to zero for both

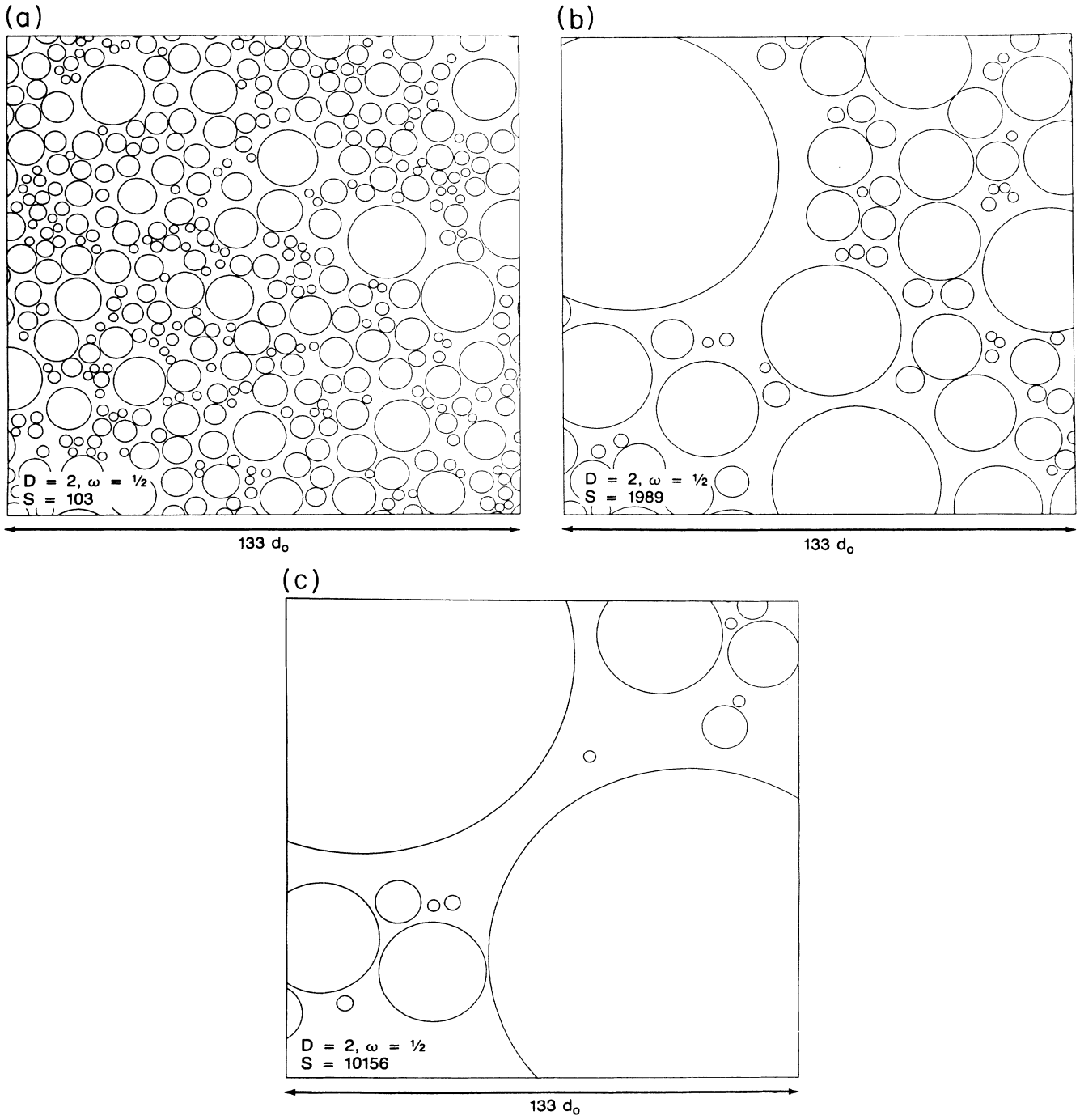

FIG. 13. Results obtained from a simulation similar to that illustrated in Fig. 12 except that the dimensionality (D) of the droplets is 2. (a)–(c) show a portion of the system at the stages at which the mean cluster size S has reached values of 103, 1989, and 10 156, respectively.

small and large values of x, the exponent z' can be obtained directly from the definition of $N(t)$ and the scaling form (5). We find

$$N(t)=\sum_s N_s(t)\sim\int ds\, s^{-\theta}f(s/S(t))\sim S^{1-\theta}\times\int dx\, x^{-\theta}f(x)\sim t^{z(1-\theta)}\ . \tag{29}$$

In comparing (29) with (4), and substituting the values of θ and z from (26) and (28), respectively, we obtain

$$z'=\frac{d}{1-\omega}\ . \tag{30}$$

Figures 18(a)–18(c) show the growth of the mean droplet size (S) and time dependence of the total number of drop-

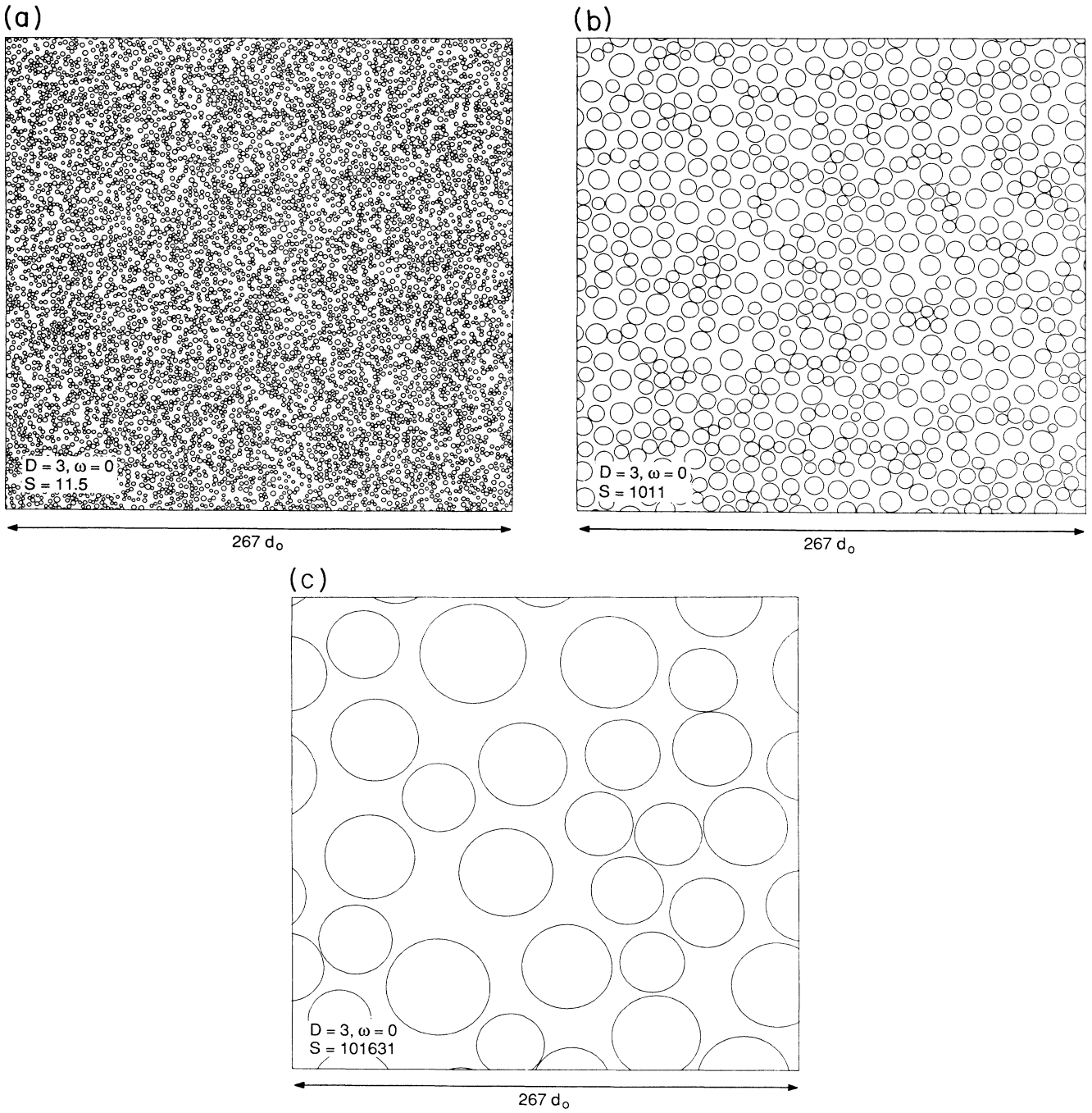

FIG. 14. Three stages in a simulation of droplet growth and coalescence. In this case, three-dimensional droplets are growing on a two-dimensional substrate with a growth exponent ω of 0. The simulation was stopped and the droplet distribution recorded at the stages corresponding to mean droplet sizes (S) of 11.5, 1011, and 101 631 in (a)–(c), respectively.

lets (N) obtained from the simulations used to generate Figures 16(a)–16(c), respectively. The slope of the lines for S and N are in agreement with the theoretical predictions $z=D/(1-\omega)$, [Eq. (28)], and $z'=d/(1-\omega)$, [Eq. (30)], respectively.

The effective values obtained for the exponents z and z' are listed in Table II. The theoretical values obtained from (28) and (30) are given in parentheses. In all cases we have obtained the best scaling plots of the droplet size distributions using the theoretical value for θ from (26).

C. Kinetic equation approach for heterogeneous nucleation

We can apply the kinetic equation (17) to heterogeneous nucleation, but here $K'_{i,1}$ is the rate of growth of droplets of size i according to (22), which is the growth rate due to absorption of monomers. Using the same scaling transformations as in (18) we find

$$\theta-\frac{1}{z}=1+\lambda \ . \tag{31}$$

In addition, the coefficient $K'_{s,1}$ is given by the rate of growth of the droplets, namely

$$K'_{s,1}\sim\frac{ds}{dt}\sim s^{\nu}, \quad \nu=\frac{\omega+D-1}{D} \ . \tag{32}$$

Therefore the kinetic equation gives the same expression (28) for the growth exponent z. Substituting the exact values of θ and z from (26) and (28), respectively, in (31) we find

$$\lambda=\frac{\omega+d-1}{D} \ . \tag{33}$$

We are not aware of any derivations of (33). However, since (33) reduces to (21) for a special value of ω (see Sec. IV), it should be possible to use a unified approach to determine the degree of homogeneity of the kernel for both the homogeneous and the heterogeneous nucleation models.

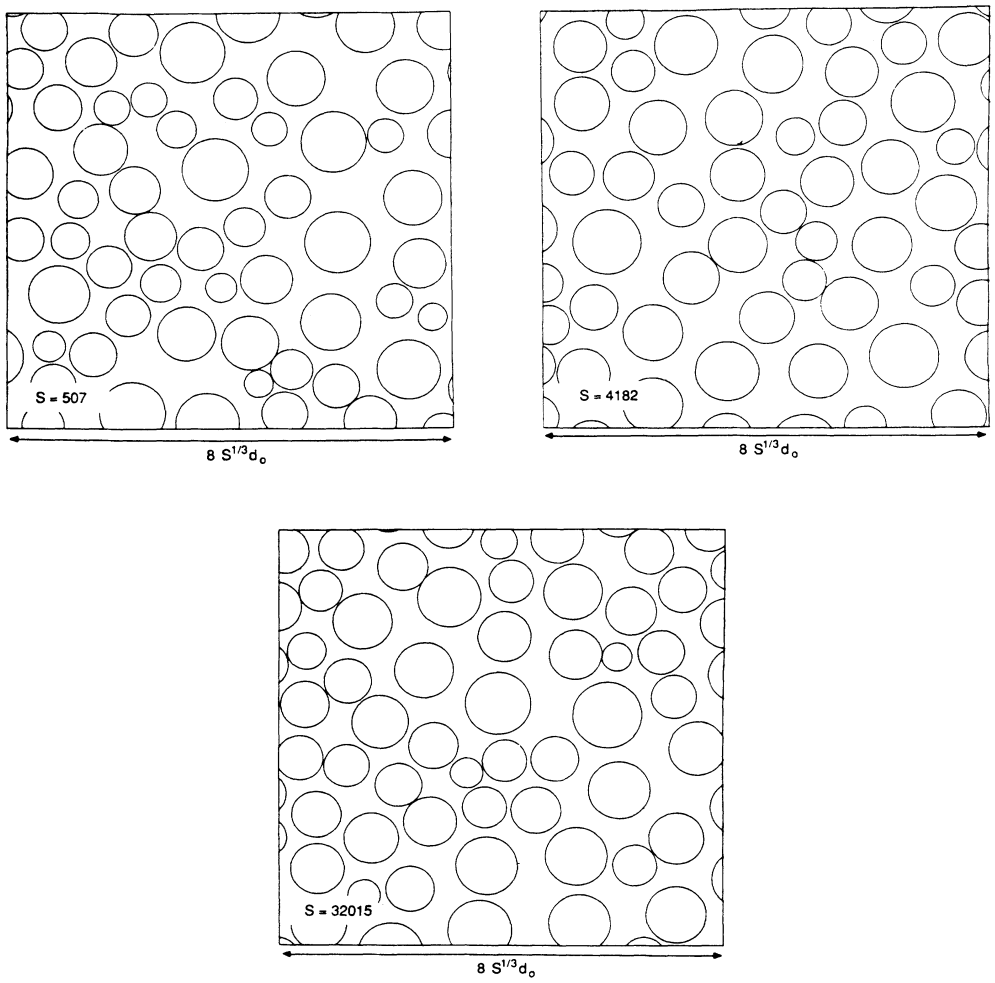

FIG. 15. Results taken from a simulation of droplet growth and deposition for the case $D=3$, $d=2$, and $\omega=0$. The system is shown at three stages ($S=507$, 4182, and 32 015) on scales proportional to $S^{1/3}$ ($S^{1/D}$). This figure illustrates the scaling properties of the system and the self-similarity of the droplet size distribution at different times when the length scale is rescaled by $S^{1/D}$.

IV. DISCUSSION

A. Comparison with homogeneous nucleation

We now compare and contrast heterogeneous droplet growth with homogeneous nucleation. The growth of large droplets in homogeneous nucleation is governed by the rate at which a droplet absorbs small droplets from the vapor. Assuming a uniform vapor density, the rate of growth of the volume of the droplets is proportional to their area, i.e.,

$$\frac{d(R^D)}{dt} \propto R^d . \tag{34}$$

This implies that $R \sim t^{1/(D-d)}$. In comparing this result with (27), we find that $\omega = 1 - D + d$ for the growth of large droplets in homogeneous nucleation. Substituting this value of ω in (28) we find $z = D/(D-d)$, in agreement with (14). The same result is found if we substitute the value $\omega = 1 - D + d$ for homogeneous nucleation in (32). In this way, again we find

$$\lambda = \frac{2d}{D} - 1 , \tag{35}$$

in agreement with (21).

The main difference between homogeneous nucleation and heterogeneous nucleation is the continuous replenishment of monomers and small droplets in the case of homogeneous nucleation. This is reflected in the appear-

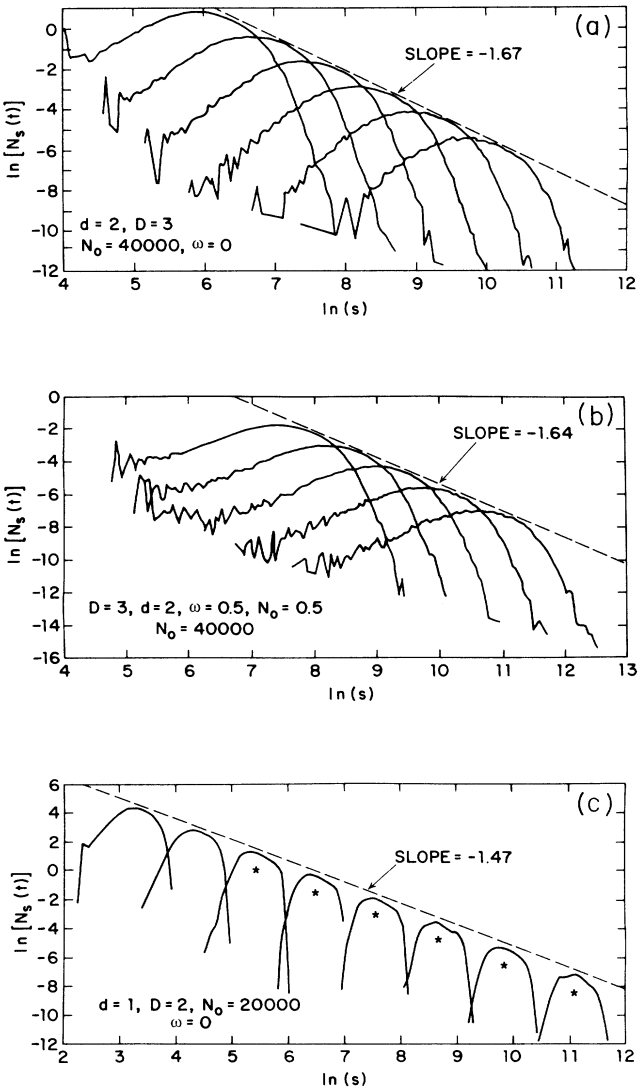

FIG. 16. Droplet size distributions obtained from three different models for heterogeneously nucleated droplet growth and coalescence. (a) and (b) show results from simulations with $D = 3$ and $d = 2$ with growth exponents ω of 0 and 0.5, respectively. (c) shows the distribution for simulations with $D = 2$ and $d = 1$ with $\omega = 0$.

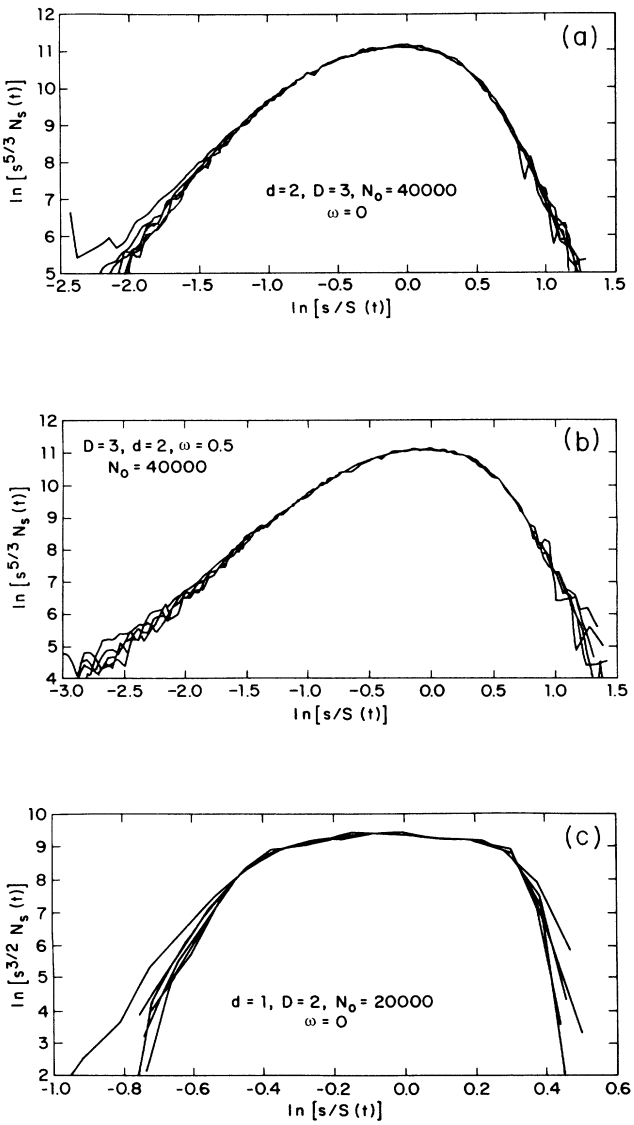

FIG. 17. Scaling of the droplet size distributions shown in Fig. 16. The scaling form given in Eq. (5) was used with a scaling exponent θ of $(D+d)/D$ [Eq. (26)].

ance of two types of size distributions in the homogeneous nucleation system: a power-law decay at small sizes, indicating a polydispersed distribution, superimposed on a bell-shaped curve at larger droplet sizes. The bell-shaped distribution arises from the growth and coalescence of large droplets. The polydispersed part of the distribution, which does not exist in the case of heterogeneous nucleation, is due to the continuous feeding of the monomers and nucleation of small droplets. The fact that a source of particles leads to the formation of a steady-state power-law size distribution was recognized already in the case of cluster-cluster aggregation in the presence of a source and a sink.[25]

In order to show that the bell-shaped part of the distributions in both models have the same origin, in Fig. 19 we have plotted the scaled distributions for the case of homogeneous and heterogeneous nucleation models. The graphs show that, in fact, the distribution of large droplets in the two models are quite similar, indicating that these droplets form by the growth and coalescence process. In contrast, the feeding of small droplets and their homogeneous nucleation leads to the formation of the polydispersed part of the distribution in the homogeneous nucleation process.

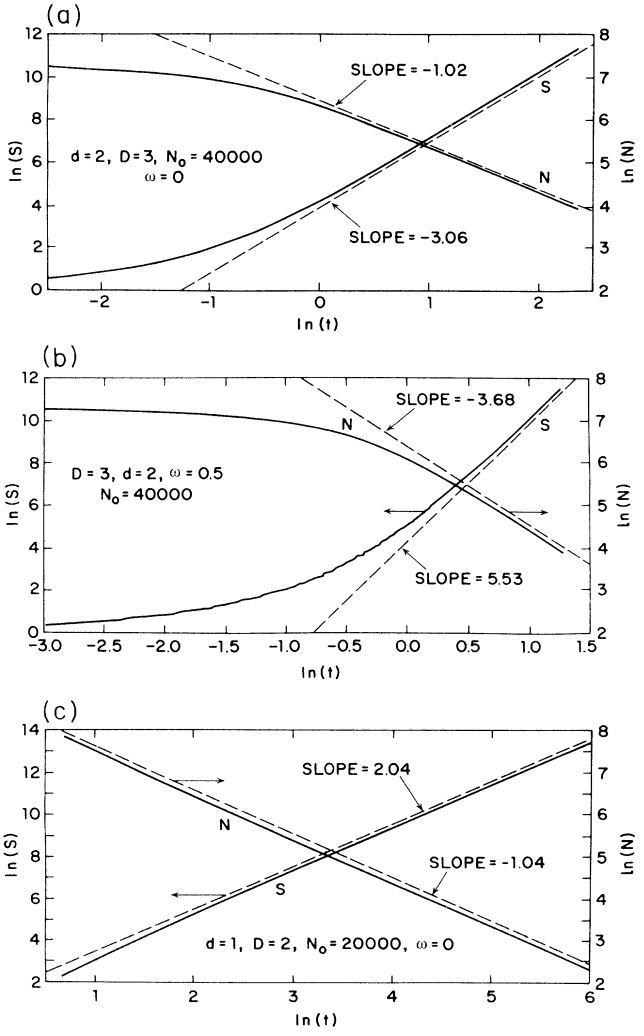

FIG. 18. (a)–(c) show the growth of the mean droplet size S and time dependence of the total number of droplets N obtained from the simulations used to generate Figs. 16(a)–16(c), respectively. The slope of the lines for S and N are in agreement with the theoretical predictions $z=D/(1-\omega)$, [Eq. (28)], and $z'=d/(1-\omega)$, [Eq. (30)], respectively.

TABLE II. Effective values obtained for the exponents z and z' from the droplet growth and coalescence models (heterogeneous nucleation model). The theoretical values are given in parentheses. In all cases a convincing data collapse of the droplet size distributions could be obtained using the theoretical values for θ ($\theta=1+d/D$).

d	D	ω	z	z'
1	1.5	0	1.59 (1.50)	1.05 (1.0)
1	1.5	0.5	3.4 (3.0)	2.35 (2.0)
1	2	−0.5	1.38 (1.33)	0.68 (0.67)
1	2	0	2.04 (2.0)	1.04 (1.0)
1	2	0.5	4.11 (4.0)	2.07 (2.0)
1	3	−1	1.50 (1.50)	0.50 (0.50)
1	3	−0.5	2.02 (2.0)	0.67 (0.67)
1	3	0	3.03 (3.0)	1.02 (1.0)
1	3	0.5	6.22 (6.0)	2.11 (2.0)
1	4	0.5	2.71 (2.67)	0.65 (0.67)
1	4	0	4.03 (4.0)	1.02 (1.0)
2	3	−1	1.57 (1.50)	1.01 (1.00)
2	3	−0.5	2.06 (2.0)	1.40 (1.33)
2	3	0	3.06 (3.0)	1.02 (1.0)
2	3	0.5	5.72 (6.0)	3.87 (4.0)
3	4	−1	2.30 (2.0)	1.67 (1.50)
3	4	0	4.43 (4.0)	3.35 (3.0)
3	5	−1	2.64 (2.50)	1.55 (1.50)
3	5	0	5.02 (5.0)	2.95 (3.0)

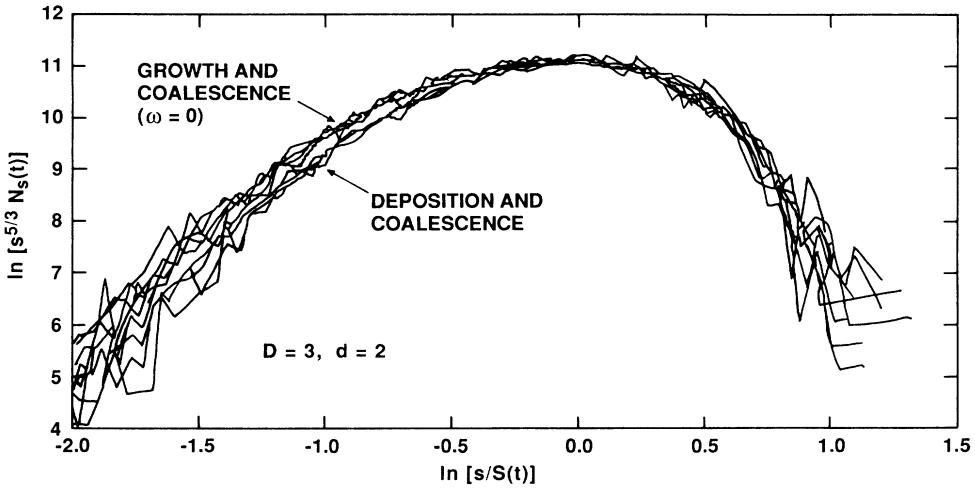

FIG. 19. Scaling of the large droplet part of the size distributions in the deposition and coalescence (homogeneous nucleation) and growth and coalescence (heterogeneous nucleation) models. The similarity of the two distributions is quite evident and points to the conclusion that the large droplets part of the distribution in the homogeneous nucleation model arise from growth and coalescence of similar size droplets.

B. Summary

In general, droplet formation occurs either by spontaneous nucleation or by growth from heterogeneously distributed nucleation centers, such as impurities. We introduced two models to describe these two types of processes. In the model for homogeneous nucleation, we assume that droplets can form and grow anywhere in the system at any stage during the deposition, growth, and coalescence process. This model appears to capture the essential features of the distribution of droplets in vapor deposited thin-film experiments.[1] The reason is that one can clearly observe two types of distinct distribution of droplets in the scanning electron microscope micrographs of tin deposited on sapphire [see Fig. 1(a)]. One pattern consists of the larger droplets that form a monodispersed distribution. This distribution is superimposed on a highly polydispersed distribution of smaller droplets forming the background in the micrographs. We have obtained similar bimodal distribution of droplets in our simulations of the homogeneous nucleation model. In contrast, in the case of droplet growth and coalescence from nucleation centers, there exists only a single distribution consisting of a monodispersed distribution of large droplets that evolves with time. Thus the homogeneous nucleation model appears to be a better candidate for describing the experiments on droplet growth in vapor-deposited thin films. Currently we are carrying out an extensive analysis of the experimental data and a quantitative comparison with the homogeneous nucleation model and the results will be published elsewhere.

In summary, the formation of a distribution of droplets is ubiquitous in nature, from thin films to water droplets in rain and clouds. We showed that the scaling description is an effective method for describing the kinetics of droplet growth. The reason is that any function specifying the space-time evolution of the droplet growth process can be written in a universal form by transforming the variables (r,t) into $(br, b^{D/z}t)$. This rescaling allows comparison of data from quite different systems. In addition, we developed kinetic equations for describing the evolution of the droplet size distribution and obtained expressions for the homogeneity kernel for the homogeneous and heterogeneous nucleation processes. We hope that these results will stimulate further experiments, simulations, and theoretical work and will provide a solid foundation for understanding droplet growth in diverse physical systems.

ACKNOWLEDGMENTS

We would like to thank Larry Carr and Bryan Caldwell for their experimental collaboration on the work reported in Fig. 1(a). This research was supported by the Office of Naval Research and the Research Corporation. One of us (F.F.) would also like to thank the Donors of the Petroleum Research Fund, administered by the American Chemical Society, for partial support of this work.

[1]F. Family and P. Meakin, Phys. Rev. Lett. **61**, 428 (1988).
[2]P. Meakin and F. Family, J. Phys. A **22**, L225 (1989).
[3]F. Family, in *Random Fluctuations and Pattern Growth*, edited by H. E. Stanley and N. Ostrowsky (Martinus-Nijhoff, Dordrecht, 1988), p. 345.
[4]H. Merte, C. Y. Amali, and S. Son, in *Proceedings of the Eighth International Heat Transfer Conference, San Francisco, 1986* (Hemisphere, Washington, 1986), Vol. 4, p. 1659.
[5]D. Beysens and C. M. Knobler, Phys. Rev. Lett. **57**, 1433 (1986).
[6]J. L. Viovy, D. Beysens, and C. M. Knobler, Phys. Rev. A **37**, 4965 (1988).

[7]D. Fritter, C. M. Knobler, D. Roux, and D. Beysens, J. Stat. Phys. **52**, 1447 (1988).
[8]D. Weaire and N. Rivier, Contemp. Phys. **25**, 59 (1984).
[9]A. R. Kerstein, Combust. Flame (to be published).
[10]S. Kang, J. J. Helble, A. F. Sarofim, and J. M. Beér, in *Proceedings of the Twenty-Second International Symposium on Combustion, Pittsburgh, 1988* (The Combustion Institute, Pittsburgh, 1988), p. 101.
[11]A. T. Florence, T. K. Law, and T. L. Whateley, J. Colloid Interface Sci. **107**, 584 (1985).
[12]B. J. Mason, *The Physics of Clouds* (Oxford University Press, London, 1957).
[13]J. D. Gunton, M. San Miguel, and P. S. Sahni, in *Phase Transitions and Critical Phenomena,* edited by C. Domb and J. L. Lebowitz (Academic, London, 1983), Vol. 8.
[14]M. Hennion, D. Ronzand, and P. Guyot, Acta Metall. **30**, 599 (1982).
[15]Y. C. Chou and W. I. Goldburg, Phys. Rev. A **23**, 858 (1981).
[16]G. L. Carr, B. Caldwell, F. Family, and P. Meakin (unpublished).
[17]B. Lewis and J. C. Anderson, *Nucleation and Growth of Thin Films* (Academic, New York, 1978).
[18]P. Meakin, in *Phase Transitions and Critical Phenomena,* edited by C. Domb and J. L. Lebowitz (Academic, London, 1988), Vol. 12.
[19]M. J. Stowell, T. J. Law, and J. Shaw, Proc. R. Soc. London, Ser. A **318**, 231 (1970).
[20]M. V. Smoluchowski, Z. Phys. **17**, 557 (1916).
[21]D. Stauffer, *Introduction to Percolation Theory* (Taylor & Francis, London, 1985).
[22]T. Vicsek, P. Meakin, and F. Family, Phys. Rev. A **32**, 1122 (1985).
[23]T. Vicsek and F. Family, Phys. Rev. Lett. **52**, 1669 (1984).
[24]T. Vicsek and F. Family, in *Kinetics of Aggregation and Gelation,* edited by F. Family and D. P. Landau (North-Holland, Amsterdam, 1984), p. 111.
[25]P. Meakin, T. Vicsek, and F. Family, Phys. Rev. B **31**, 564 (1985).
[26]M. Kolb, Phys. Rev. Lett. **62**, 1699 (1989).
[27]F. Family and P. Meakin, Phys. Rev. Lett. **62**, 1700 (1989).

(a)

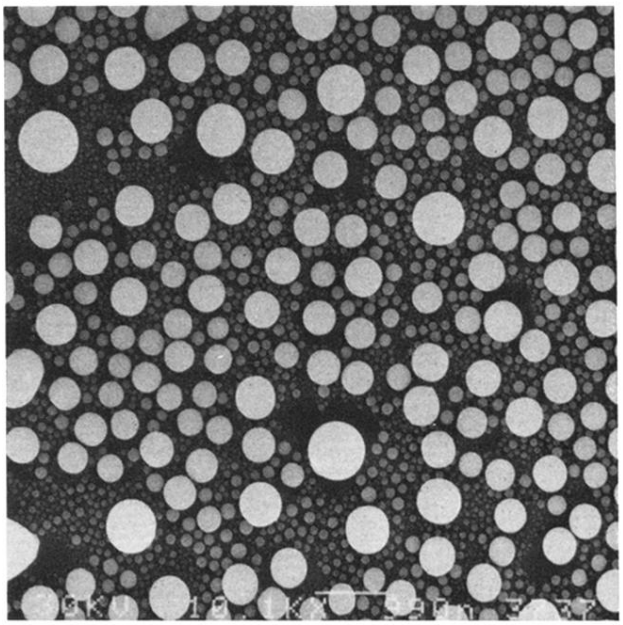

(b)

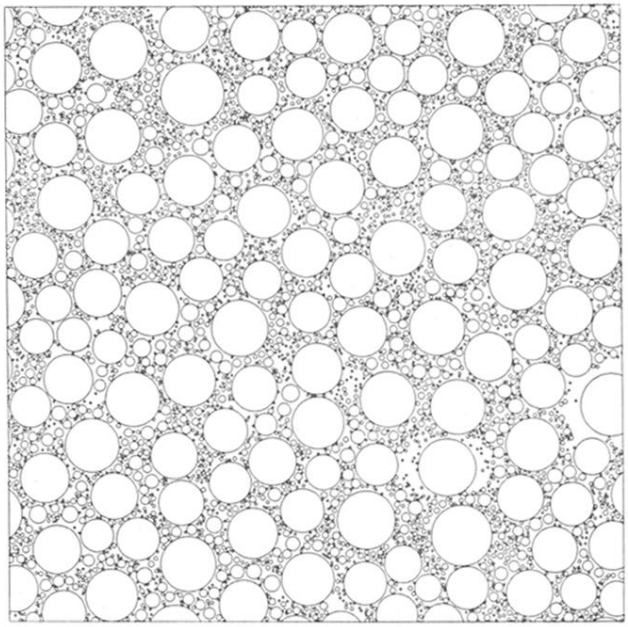

FIG. 1. (a) Comparison of an electron micrograph of tin droplets grown on a sapphire surface held at 230 °C by vapor deposition and (b) simulation carried out using the droplet deposition and coalescence model. The simulation results were obtained from a model in which three-dimensional droplets with a radius of 0.75 were randomly deposited onto a two-dimensional plane of area 512×512. The system is shown at the stage at which the mean droplet size $S(t)$ has reached a value of 1029 (in units of the mass of the deposited droplets). A 200×200 area is shown here. The uniform size of the larger droplets indicates that there exists an approximately monodispersed distribution of droplets which is superimposed on a wide distribution of smaller droplets. Depleted zones created by coalescence of droplets around large droplets are evident in both the experimental and the simulation data.